Calibration of the TFTR lost alpha diagnostic

R. L. Boivin
Plasma Fusion Center, Massachusetts Institute of Technology, 175 Albany Street, Cambridge, Massachusetts 02139

Z. Lin, A. L. Roquemore, and S. J. Zweben
Plasma Physics Laboratory, Princeton University, Princeton, New Jersey 08543

We present various aspects of the calibration of the TFTR lost alpha diagnostic. The diagnostic consists of four detectors, forming a poloidal array at the bottom of TFTR inside the vacuum vessel. The detector is composed of a ZnS(Ag) scintillator and a pair of collimating apertures which permit pitch angle, energy, and time resolution of the escaping flux of high-energy ions (MeV range). The first goal of this study was to establish the absolute calibration of the diagnostic for different particle types and energies. This enables us to compare for the first time, measured losses with loss calculations based on a first-orbit model. However, the factor of 2 uncertainty in the final calibration is still too large for full, quantitative comparisons of the data with the theory based on absolute flux measurements alone. We also present some of the aspects related to the detector's resolution capabilities, its temperature dependence, and its time response.

I. INTRODUCTION

The TFTR lost alpha diagnostic is presently composed of four detectors based on a scintillation technique. They are located at four different poloidal locations at the bottom of the vacuum vessel, inside the first wall, but at the same toroidal location (in between TF coils, bay E). The diagnostic was designed to measure losses to the walls of high-energy ions (MeV range), particularly the naturally occurring charged fusion products (1-MeV triton, 3-MeV proton, 3.5- and 3.7-MeV alphas). Three of the detectors, located at poloidal angle of $\theta \simeq 90°$, $60°$, and $45°$ below the outer midplane, are fixed to the bottom of the vacuum vessel.[1] The fourth one, located just below the midplane ($\theta \simeq 20°$), is mounted on a radially movable probe which can be inserted approximately 25 cm inside the first wall.[2]

The detector is composed of a scintillator [ZnS(Ag) also known as P-11] and a pair of collimating apertures through which high-energy particles are dispersed according to their gyroradius (energy) and toroidal pitch angle (magnetic moment). Shown in Fig. 1 is a schematic diagram of the detector and its basic components. The scintillator light pattern is then imaged through a series of lenses and coherent fiber optic bundles to a camera and photomultiplier tubes for recording. In the present configuration, roughly 10^8 particles/cm^2/s impact onto the scintillator during a TFTR discharge (at approximately $I_p = 1.0$ MA and with a total of $\sim 10^{15}$ fusion reactions per second). Due to this high flux, and in order to maintain the necessary dynamic range,[3,4] the detectors were operated in "current" mode rather than in single-particle ("pulse") counting mode.

II. CALIBRATION PROCEDURE

In order to facilitate the calibration process and to identify the contributions of various uncertainties the diagnostic has been divided in two relatively independent parts. The first part, seemingly simple, consists of the scintillator itself. Although used for decades now, the scintillation process in ZnS(Ag) is still not completely understood, although many of its characteristics can be found in the literature.[5-7] The second part consists of the optical coupling between the scintillator and the recording medium.

As mentioned above, the first step in the calibration of the diagnostic lies in the scintillator itself. Here is the list of items examined in the process:[8] (i) absolute calibration: light emission per particle, (ii) light flux versus particle energy, (iii) light flux versus particle type, (iv) light flux versus particle angle of incidence, (v) temperature dependence of the scintillation efficiency, (vi) time response of the scintillator, (viii) radiation damage (long exposures).

To this list we can add the verification of the emission linearity and of possible saturation levels at very high particle flux. This verification is still under way and the results will be reported elsewhere. One major obstacle prevented a complete *in situ* calibration of the detector, as installed within the vacuum vessel. This problem, particularly important for D-D operations, is the absence of radioactive isotopes emitting high-energy protons or tritons. Consequently, one needs to calibrate the scintillator inside an auxiliary D-D fusion generator. Another difficulty lies in the very short range of those MeV ions in air (a few centimeters), necessitating a vacuum chamber for an effective calibration.

III. SCINTILLATOR CALIBRATION

The scintillator[9] is composed of a thin layer (10–15 μm) of tiny ZnS(Ag) crystals (of approximately 10 μm in size) deposited on a 2.5 cm$\times$2.5 cm quartz substrate. Silver is added as an activator ($\simeq 120$–150 ppm) with some aluminum which acts as a coactivator. The scintillation process is largely dominated by a transition occurring at
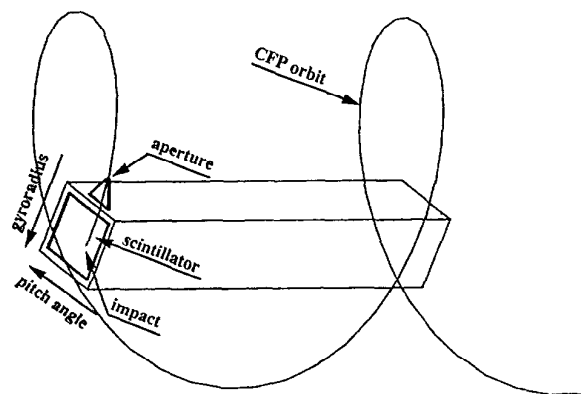
FIG. 1. Schematic diagram of the detector design. Components are roughly to scale, including a typical CFP orbit (with a gyroradius ≈ 7.5 cm and 60° pitch angle).

450 nm, in the blue region of the visible spectrum. An impacting ion should produce approximately 10^5 blue photons per MeV deposited in the scintillator, since the light emission efficiency (total light energy versus impacting ion energy) of the ZnS has been found to be of the order of 10%–20%.[10,11] The presence of many small crystals causes the scintillator to be opaque to its own light; the light emitted is reabsorbed, reflected, and redistributed within the scintillator crystals. The consequences and magnitude of the opacity will be discussed below.

The thickness of the scintillator has been measured by precisely weighting the amount of ZnS on the substrate; since the density of the ZnS is known to be 4.1 g/cm^3,[12] the averaged thickness was found to be 10 μm ± 15%. Note that this averaged thickness does not take in account the intercrystal space present in the powder.

The opacity has been measured by using an alpha source and two identical scintillators. The light emission from alpha particles was measured by a photomultiplier located at the back of one scintillator. A second scintillator was then added between the first scintillator and the photomultiplier tube. It was found that only 30%–40% of the blue light emission from the first scintillator was transmitted through the second one. This simple measurement shows that the scintillator opacity needs to be included in the complete theoretical model of the scintillator light emission efficiency.

In Fig. 2 is shown the setup for the scintillator calibration. On one side is the ion beam itself (Cockcroft–Walton type), capable of voltages up to 150 kV (and with some simple modifications up to 200 kV) and beam currents up to a few milliamperes. Magnets could be put in the accelerator section in order to remove the half and third energy components of the beam ions, but they were not used in order to maximize deuterium loading of the target. The target chamber, with a diameter of 45 cm and a depth of 15 cm, contained the target and the different detectors. The target was made of titanium (a 1-cm-diam, 0.6-cm-thick "butt") and was simply attached to a movable holder with-
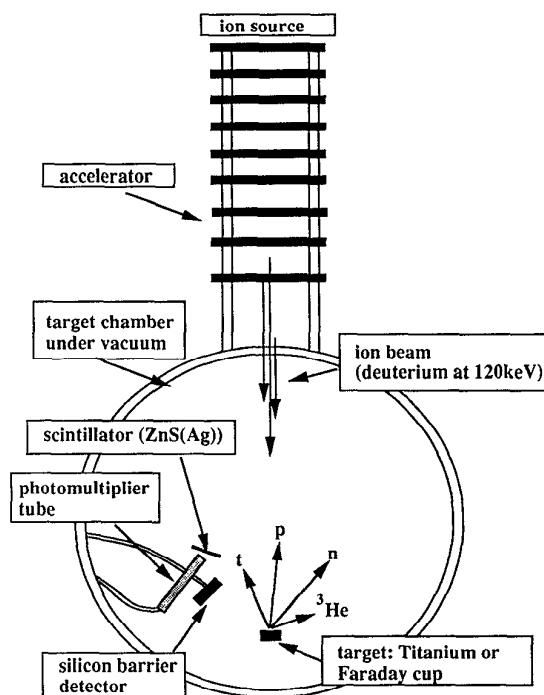

FIG. 2. Schematic diagram of the experimental setup for the scintillator calibration.

out active cooling. Titanium was chosen for its good deuterium retention.

The detectors were located close to the target (typically 10 cm or so) in order to maximize the count rate. The silicon barrier detector (or surface barrier diode, SBD) was installed next to the scintillator for flux and energy calibration of the charged fusion product source. The SBD was itself energy calibrated by using an ^{241}Am alpha source with a 4.5 ± 0.3-MeV peak energy (after a gold foil present on the source). Next to the SBD, the scintillator was installed facing the target at an angle of 15°–20°, simulating the angle of incidence used in the TFTR detectors. A photomultiplier tube[13] (~ 1.8-cm diameter) was installed very close to the scintillator in order to maximize photon collection. Signals were then transmitted by feedthroughs to preamplifiers located outside the chamber. The energy of CFPs was changed by putting aluminum foils of different thicknesses (from 0.8 to 59 μm) in front of both the SBD and the ZnS(Ag).

Because of the relatively low production rate of charged fusion products (globally, approximately 10^6 fusion reactions per second), these measurements were made in the pulse count mode (typically 10^3 counts/s/cm^2) as opposed to the "current" mode (typically 10^8 counts/s/cm^2) used in the actual setup in TFTR. It is assumed here that the scintillator light output per particle would remain the same in both modes (except, for possible saturation of the scintillation process, estimated to be important only at very high particle flux [$\gtrsim 10^{11}$ counts/s/cm^2]).

Shown in Fig. 3 is a typical pulse height spectrum for the SBD and for the photomultiplier tube looking at the
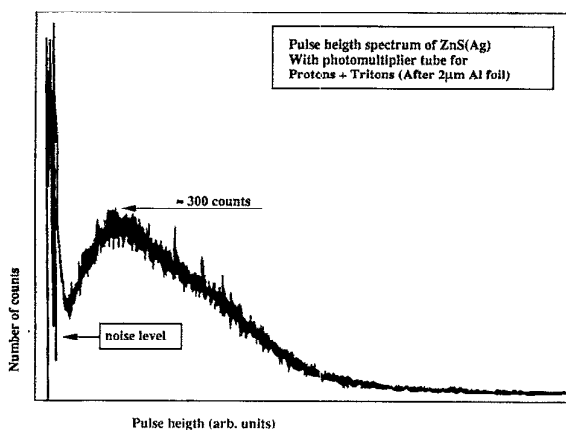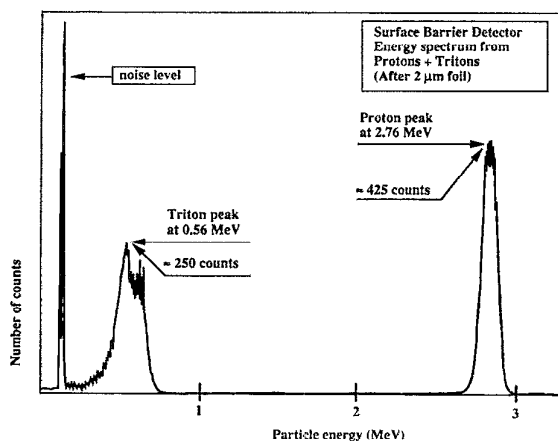
FIG. 3. Typical pulse-height spectra for the silicon barrier detector (top) and for the photomultiplier tube (bottom) coupled to the scintillator. In this case, a 2-μm aluminum foil was used in front of the detectors. Large levels at low pulse heights are due to detector noise.

FIG. 4. Particle ranges in ZnS(Ag) for the triton, proton, and alpha vs their incident energy.

scintillator. In this case, a 2-μm aluminum foil was used in front of the detectors. Attention needs to be drawn to the SBD spectrum [Fig. 3(a)], where the effect of the beam-induced Doppler shift of the particles energy is visible. The peak energy of the protons is 2.76 MeV, down-shifted from the center of mass birth energy of 3 MeV (in this case a 3-MeV proton loses only 50 keV through the 2-μm Al foil). In fact, since the detectors are located at an angle of approximately 45° on the beam side, the triton energy would be reduced by up to 25% (and somewhat less for the proton).[14,15] The 0.8-MeV ^{3}He is stopped by the thin aluminum foil except at the thinnest foil (0.8 μm) where it is barely visible on the SBD energy spectrum.

Shown in Fig. 3(b) is the scintillator photon pulse height spectrum. The reasons for a broadened light spectrum are multiple. First, the scintillator is composed of many small crystals with an irregular granular structure; impacting ions hit only part of a given crystal. Second, the scintillator is opaque to its own light; only some part of the light will reach the photomultiplier tube. Third, some fraction of the light is reflected and refracted [ZnS(Ag) index of refraction is 2.356] many times in the crystals. Fourth,
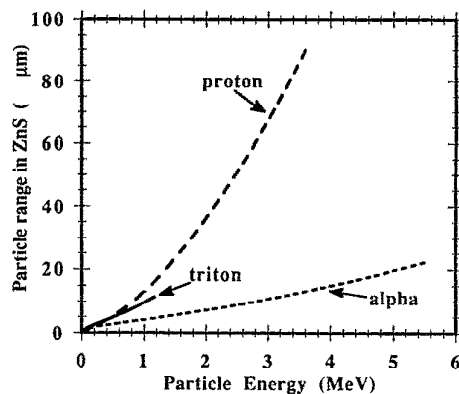
we expect the light emission efficiency to be a function of the particle type (also known as the α/β ratio).[12,16–18] And finally, the 3-MeV proton is not fully stopped in the scintillator. Consequently, since the spectrum could not be used in separating the different species contribution, the difference in light response due to the protons and the tritons was determined by exploiting their different range in aluminum. By using thicker aluminum foils (thus stopping the triton but not the proton), it was possible to isolate the individual proton and triton contributions.

A. Scintillator light emission versus particle energy and species

For a given type of particle, the light emission of the scintillator is, as a first approximation, proportional to the amount of energy deposited in the crystals.[19] This approximation is especially good for inorganic scintillators [e.g., ZnS(Ag)] and for the range in energy of interest (MeV range). By using the tables of stopping power in materials edited by Andersen and Ziegler,[20,21] we can calculate the amount of energy deposited by MeV ions in ZnS. Conversely, we can calculate the range of a given particle in the scintillator as a function of its energy.

In Fig. 4 is shown the calculated range of pertinent energetic particles in ZnS versus their energy. Note the relatively long range of the 3-McV proton compared to the 1-MeV triton. The main factors behind the need for a complete experimental calibration, specialized to our diagnostic configuration, are the absence in the literature of an absolute light efficiency for the ZnS(Ag) (which is also dependent on the thickness), the different particle ranges in the scintillator, the different light efficiency for each particle, and the scintillator opacity.

Some of these factors determine the choice of a very thin scintillator, around 10 μm. At this thickness a maximum of light could be obtained from the interaction of charged fusion products with the scintillator.[22] The MeV ions are nearly fully stopped and the opacity of the scintillator is kept to a minimum. The choice of a thin scintillator had also the definite advantage of minimizing gamma and neutron scintillation,[3,4] leaving the x rays (originating

from the plasma and from reflections on the walls) as a background concern. The latter can be eliminated by shielding the scintillator with at least 3 mm of stainless steel[1] or 1 mm of tantalum or tungsten.

The energy and particle species dependence of the scintillator light emission were studied together in the target chamber (see Fig. 2). The absolute calibration of the scintillator will be based on the light response from a known source of alpha particles. The light emission from alpha particles (from the ^{241}Am source) will be compared to that from protons and tritons and to an absolutely calibrated light source. We will then have the absolute value of the light emission of the ZnS(Ag), 10-μm thick, from the exposure to MeV ions in a geometry similar to the one used in the TFTR detectors.

In Fig. 5 is shown the experimentally measured dependence of the total (integrated over all pulse heights, noise removed) scintillator light emission versus proton, triton, and alpha energy. All three graphs use the same vertical scale and so the light emission from the three different particle types can be compared directly. The light emission of the ZnS(Ag) is given as a function of the particle energy prior passing through a 3-μm Al foil as used in our detectors. The different contribution of protons and tritons was established by using the thinnest foil which would stop the tritons completely, in this case a 10-μm Al foil. Since protons lose a small or negligible amount of energy through a foil of 10 μm or less (< 10%), their contribution to light emission was considered to be constant (see Fig. 5) for all cases with foils thinner than 10 μm. The triton contribution was thus established (with foils thinner than 10 μm) as being any additional light emission above the 10-μm Al foil case, which consisted of the proton contribution only.

The experimental curves are compared with a very simple model which calculates the total amount of energy deposited in the scintillator. All the model curves are vertically normalized so that for a particle with no energy after the foil, the scintillator response would be zero. The curves are also normalized with the experimental results at the highest energy point. The difference between the two curves exemplifies the effects of opacity, which will be briefly discussed below.

The light response of the scintillator to different particles at their birth energy can be obtained directly from Fig. 5. The 3-MeV proton gives, in that geometry, 1.5±0.2 more light than a 1-MeV triton, whereas the 3.5-MeV alpha would give approximately 8.0±2.0 times more. Recall that these energies correspond to the particles energy before they go through the detector's 3-μm aluminum foil. This result is very important for D-D operations; it implies that ~60% of the light signal is due to protons (and so 40% to tritons) contrary to what was previously estimated.[1,2,4,23] The physical causes for these ratios are multiple and will be discussed below.

First, after passing the 3-μm Al foil located in the detector, the triton energy is only ≃0.7 MeV, whereas the proton energy is still close to 3 MeV. Then the particles impact on the scintillator at an angle of 15°–20°. At that angle the scintillator has an effective thickness of 30–40
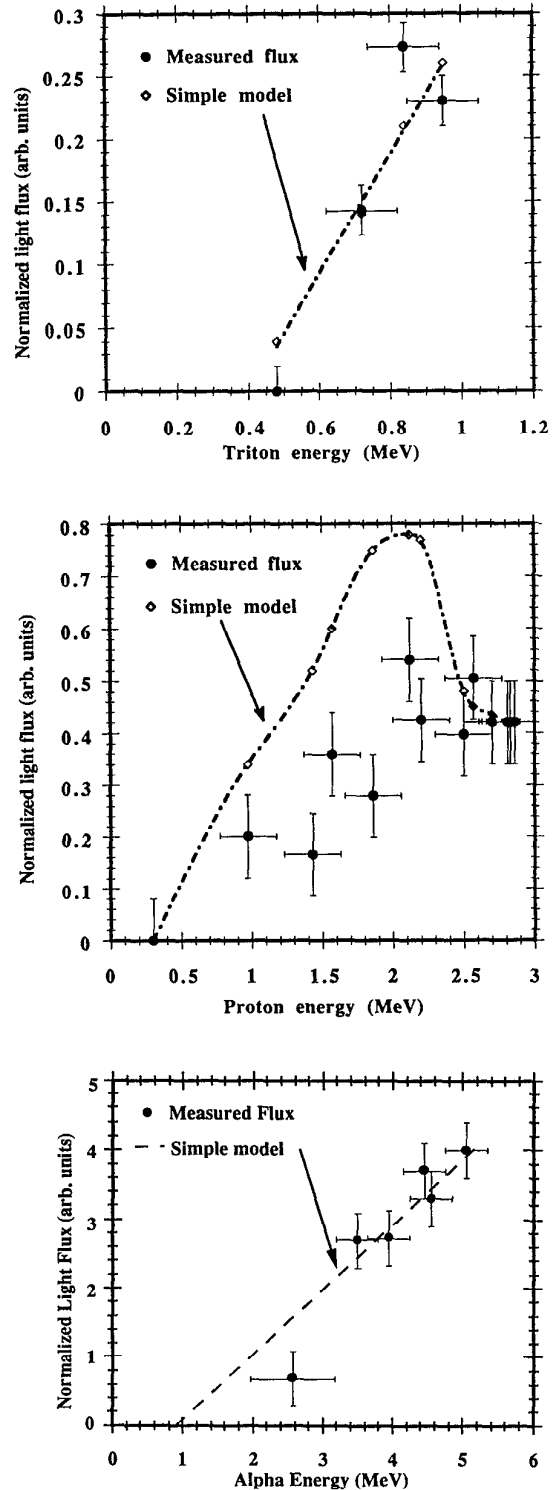

FIG. 5. Measured and calculated energy dependence of the scintillator for tritons (top), protons (middle), and alphas (bottom). The three experimental curves are based on the same vertical scale.

μm, compared to the 10 μm seen by a normally incident particle. In that situation the 3-MeV proton would deposit approximately 2.2 MeV of its energy and the triton all its 0.7 MeV. However, a larger fraction of the proton energy
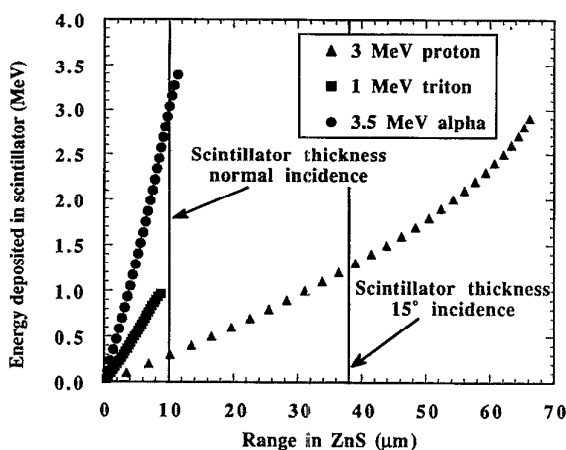
FIG. 6. Calculated energy deposition for various particle species as a function of the scintillator thickness. Particles have an incident energy corresponding to their fusion birth energy (1-MeV triton, 3-MeV proton, and 3.5-MeV alpha).

FIG. 7. Angle of incidence dependence of light emissivity to 4.5-MeV alphas for ZnS(Ag). The top points include a $1/\cos\theta$ correction for the difference in solid angles.

would be deposited in the further half of the scintillator, defined as the back side (away from the photomultiplier tube or camera). The particle stopping power peaks at lower energy (around 1 MeV for the proton) causing the unequal deposition of energy. On the other hand the triton deposits its energy very near the surface because of its small range ($\simeq 10\ \mu m$) in ZnS. The energy deposited by different particle species as a function of the ZnS thickness is illustrated in Fig. 6. We see that only the proton is not fully stopped, even with a 15° incidence angle. In addition, since the scintillator is opaque to its own light, a fraction of the light produced by the protons would not reach the front surface, explaining at least qualitatively the ratio of 3–2 obtained above.

In the case of a 3.5-MeV alpha particle, it is stopped very quickly in the scintillator with a similar range (see Fig. 4) as the 1-MeV triton (mainly because of its double charge). However, when we compare the measured light flux ratio from alphas to tritons (8 to 1) with the ratio of their energy after the foil (2.9-MeV alpha to 0.7-MeV triton) we see that the factor of 8 found above is higher that what would be expected from just considering the amount of energy deposited. This behavior (α/β ratio) has been observed previously in other scintillators (e.g. NaI, CsI)[12,16–18] but it is still not completely understood.

One other consequence of the measurement of light emission ratios concerns the eventual operation of these detectors during the D-T phase of TFTR. From this experimental measurement, it is expected that for each D-T 3.5-MeV alpha particle would give 3.6 ± 1.0 times more light signal than each D-D 3-MeV proton and 1-MeV triton combined.

B. Angular dependence

The observed light emission from the scintillator can be subject to variations depending on two different angular aspects. The first aspect is 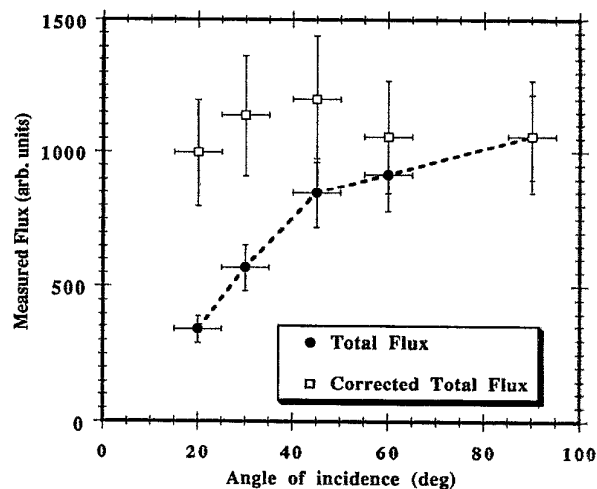related to the angle at which the camera or the photomultiplier tube records the light emission. The second corresponds to the angle at which particles impact on the scintillator. Recall that in the TFTR detectors the camera views the scintillator at a normal angle on the crystal side, which is the front side (as opposed to the quartz substrate side, defined as the back side). Particles impact on the scintillator at an angle of 15° to 20° to the surface.

When comparing the light emission from the back and the front side, effects due to the scintillator opacity and particle ranges were implicitly measured. The front to back ratio was measured by positioning the scintillator at an incidence angle of 45° with respect to the flux direction of 4.5-MeV alphas. The photomultiplier tube was positioned also at 45° (but perpendicular to the flux of alphas) and recorded the light emission from the front and back side of the scintillator in separate experiments. It was found that the front side was 1.8 ± 0.3 times brighter than the back one (for 4.5-MeV alphas). Note that since the photomultiplier was looking with a 45° angle, an additional correction is necessary since the photomultiplier tube looked at the scintillator with a 20° angle during the particle energy scan. The light emission of the scintillator was therefore compared using the photomultiplier tube at angles of 45° and 20°. After taking into account the difference in solid angles for the viewing and particle incidence angles, the ratio (front view, 20°/45°) was found to be $0.9 \pm 50\%$.

The light emission dependence on the particle angle of incidence was measured in a similar way. The photomultiplier tube was positioned directly behind the scintillator (back side). The source of alpha particles was positioned at different angles, but the relative distance between the scintillator and the source was kept the same. Shown in Fig. 7 is the angular dependence of the light emission for the ZnS(Ag) to 4.5-MeV alphas. One curve shows the raw data and the second with a $1/\cos\theta$ correction for the difference in solid angle at the scintillator.

TABLE I. Relative optical efficiency of the four detectors. The "bottom" detector ($\theta = -90°$) is taken as the reference. The poloidal angle is measured from the outer midplane.

	Detector No. 6	Detector No. 9	Detector No. 11	Midplane det.
Detector Poloidal angle (θ)	$-90°$	$-60°$	$-45°$	$-20°$
Relative efficiency	1	0.5 ± 0.1	0.64 ± 0.08	0.25 ± 0.04

Note that we cannot, at least at this stage, generalize the results of this section to other particle energies and species. A combination of effects due to the different types of particles, their different energy deposition, and the scintillator opacity prevent such a generalization.

IV. OPTICAL CALIBRATION

The second step in the calibration of the detectors (the three at the bottom and the one at the midplane) consisted of replacing the scintillator (with the detectors still inside TFTR vacuum vessel) by a known and reproducible source of light. The light pattern and intensity was recorded by the camera[24] and digitized by the PC video board[25] with the same setup used during plasma operations. The light box was made of an halogen lamp (30 W), a white diffuser,[26,27] and a blue filter, both of which were positioned approximately 25 cm away from the lamp for light uniformity.

The recorded intensity from the light box was later compared to the luminosity of the scintillator with the ^{241}Am alpha source. The direct use of the alpha source in the vacuum vessel was not feasible because of radioactive materials handling difficulties. The light box, the scintillator with the alpha source, and a commercial calibrated source of light[28] were positioned 30 cm away from a Xybion camera.[29] It was found that the light box was 3.3 $\pm 30\%$ brighter than the scintillator with the alpha source. At the same time, the scintillator emission was compared to the calibrated source of light. The spectral radiance of the light source is known to be 4.3×10^{-9} W/Sr/nm/cm^2 at $\lambda = 450$ nm. We used a blue filter (centered at 450 nm) with a 59% coefficient of transmission and a 86-nm square bandwidth. This radiance corresponds to a flux of 4.9×10^{11} (blue) photons/s/Sr/cm^2. By normalizing this radiance by the number of impacting alphas, we found that there were $2.3 \times 10^5 \pm 25\%$ (blue) photons/(4.5 MeV) alpha. This photon production (consistent with the estimate found at the beginning of Sec. III) corresponds to a scintillation energetic efficiency of 14%, consistent with the quoted efficiencies found in the literature.[10,11]

Shown in Table I is the relative optical efficiency of the different detectors at the bottom of TFTR. This cross calibration was obtained by moving the light box, with the same intensity, to the different detectors inside the vacuum vessel and by recording the light intensity with the camera. The relative poloidal distribution of escaping flux can thus be inferred by comparing the measured flux of particles from the array of detectors.

TABLE II. Description of the calculations for the absolute calibration of the midplane detector with the corresponding uncertainties. The absolute calibration corresponds to 10% full camera scale with a 10-ms integration time.

4.5-MeV alpha source strength	$2.1 \times 10^6 \pm 25\%$ alphas/cm^2/s
Light box intensity factor	$3.3 \pm 30\%$
Alpha to triton+proton ratio	$5.7 \pm 28\%$
Camera viewing angle correction	$0.9 \pm 50\%$
Particle angle of incidence correction	$1.1 \pm 18\%$
Scintillator front to back emission ratio (45°)	$1.8 \pm 18\%$
Absolute calibration (midplane detector)	$7.1 \times 10^7 \pm 75\%$ $(t+p)$/cm^2/s

Preliminary measurements of the camera stability have been undertaken during the 1990 run period. In the camera field of view, next to the scintillator's images, four "guide" lights are placed which were made of red light emitting diodes (LEDs). Assuming that the intensity of the LEDs remained constant over time, we found that the camera sensitivity did not change over a two month period (mid August–mid October) within a 20% uncertainty.

V. ABSOLUTE CALIBRATION

The absolute calibration of the diagnostic relies first on a calibrated source of alpha particles, in this case the ^{241}Am. The source strength was calibrated by using a surface barrier diode (SBD). The source was positioned at 2.5 cm from the detector behind a pinhole mask (0.16 cm in diameter). The flux through the pinhole was found to be 780 ± 20 alphas/s. The global source strength of the source was then calculated by assuming an isotropic distribution (point source) of particles, assumption later checked and found to be reasonably accurate. Integrated over one hemisphere the source was found to give $1.6 \times 10^6 \pm 20\%$ alphas/s, a number consistent with the manufacturer's strength original measurement. When the source is placed directly next to the scintillator, the flux of particles is consequently $2.1 \times 10^6 \pm 25\%$ alphas/cm^2/s.

Now we have virtually all the ingredients for providing an absolute calibration of the diagnostic. By using Table II, the complete calibration process can be retraced. The absolute light emission from the scintillator (with 4.5-MeV alphas) has been measured through the optical setup using a known source of light (with light box; Table II, first and second items). In this setup, on the bench, the camera[29] viewed the scintillator from the back and the alphas were impacting normally on the scintillator. Consequently, the level recorded for the scintillator had to be corrected, by a factor of $1.7 \pm 55\%$, which corresponds to the last three items in the table. The third factor is the translation from the 4.5-MeV alpha to the 1-MeV triton + 3-MeV proton.

By combining these factors, it was found that for a recorded light level of 10% of the camera full scale, using
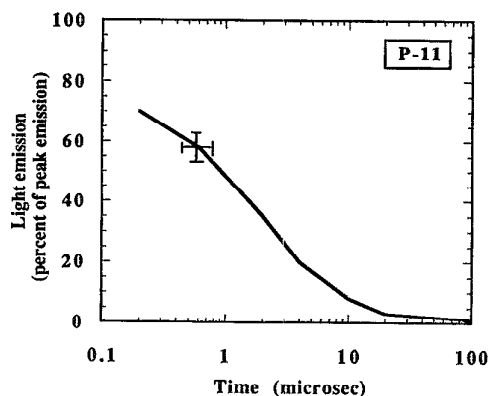
FIG. 8. Time evolution of the light emission from the ZnS(Ag) under a single excitation (single pulse). The light emission drops below 10% of the peak level (not shown here but which corresponds to a level of 100 at $t=0$) in less than 10 μs.
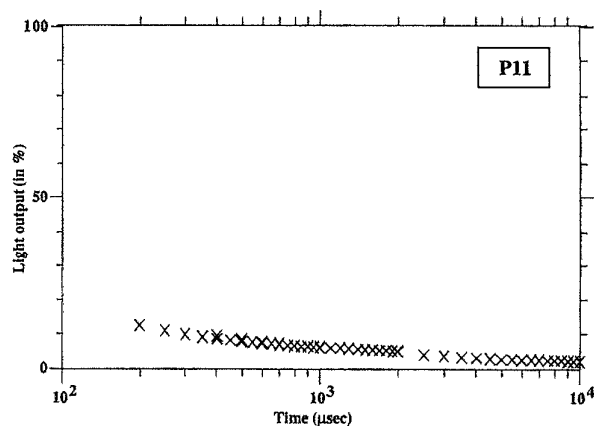

FIG. 9. Time evolution of the light emission from the ZnS(Ag) under multiple excitations. The light emission drops below 10% of the peak level ($=100$ at $t=0$) in less than 1 ms, indicating the presence of a slower time constant.

a 10-ms integrating time, there is (for the midplane detector) $7.1 \times 10^7 \pm 75\%$ (tritons+protons)/cm^2/s.

VI. TIME DECAY

Another important characteristic of the scintillator is its decay time constant. Since the scintillator can undergo de-excitation through many different processes, the light emission has several time constants which can range from a fraction of microsecond to a few milliseconds or longer.[5-7,10]

The single alpha particle excitation of ZnS(Ag) was measured using a fast triggering oscilloscope (Tektronix 7854) which can memorize and add many single excitations. Shown in Fig. 8 is the time evolution of the light from a P-11 scintillator after a single excitation with a series of 4.5-MeV alphas. The scintillator's fluorescence time decay of 1 e-folding was found to be around 2 μs (Ref. 30) with a decay to 10% of the peak level in approximately 10 μs.

The phosphorescence process (slow decay components) emerges through the trapping of electrons in the crystals which are released in a time scale of typically a few milliseconds or more. When released, the electrons recombined rapidly through a radiative decay (i.e., light emission). The slow decay components are too small to be seen on a single particle experiment due to noise in the photomultiplier tube. Another test was thus performed, but this time made with a much larger flux of alphas ($\approx 10^7$ counts/s/cm^2). For that purpose, a rotary chopper was inserted between the alpha source (^{244}Cm) and the scintillator. Shown in Fig. 9 is the time evolution of the light emission after the cessation of a large flux of incident particles. It was found[30] that the ZnS(Ag) slow time constant is such that the light emission decays to 10% of the peak level in ≈ 300 μs after the flux of particles was cut by the chopper. Standard measurements made with electron beams yielded an overall time constant of ≈ 50 μs.[11]

The different time constants found in these two experiments can be qualitatively explained as follows. Multiple excitation of the phosphor over periods longer than the fast decay time (i.e., > 1 μs) results in a cumulative build-up of the slow decay component in the average signal. Thus, when the excitation stops, the decay rate is dominated by the slow decay component. For application to the current-mode detectors on TFTR, this slow decay component will determine the dominant frequency response, which is therefore about 10 kHz. However, measurements of the relative luminance of the fast and slow components are needed for a more precise characterization of the time response of the detector.

VII. TEMPERATURE DEPENDENCE

It has been known for quite some time that the ZnS(Ag) or P-11 decreases in emission efficiency at a temperature above ~ 100 °C.[5-7] This behavior can severely limit the use of this scintillator in a harsh environment like the first wall of a tokamak where temperatures could reach several hundred degrees Celsius.

The light response of the ZnS(Ag) to alpha excitation has been measured for different scintillator temperatures.[30] The scintillator was put on the surface of a hot plate and heated up to approximately 400 °C. The source of alphas (^{244}Cm) was located at approximately 0.5 cm (in air) from the scintillator, and the light emission was recorded using a photomultiplier tube. The scintillator temperature was measured by a thermocouple. Shown in Fig. 10 is the measured temperature dependence for the ZnS(Ag) (type P-11) and also for the ZnS(Cu) (type P-31). The P-11 response is relatively flat until ~ 150 °C above which it is decreasing rapidly. This quenching effect is still not completely understood[5,6] although it is widely believed that this effect is due to decrease in the energy gap between the ground and excited states. This decrease in the gap would lead to nonradiative transfer of energy, for example by dissipating heat in the crystal structure.[30] Therefore, this regime in P-11 must be avoided (by carefully monitoring the temperature) or a more thermally stable scintillator,
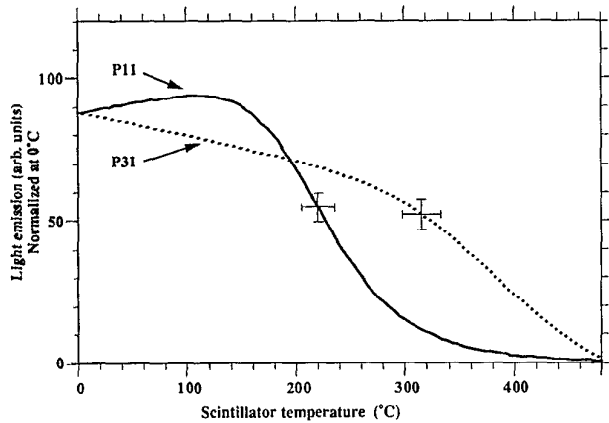
FIG. 10. Temperature dependence of the light emission for the ZnS(Ag) and for comparison, for the ZnS(Cu) (Ref. 30).

like P-31, may be used (which however has a lower light efficiency and a longer slow time decay component than P-11). Note that when heated, the scintillator is not damaged, at least not below 500 °C;[30] when returned to normal temperature the light response returns to its original value. Because of this restriction, detectors have to be well protected against the plasma heat flux or be actively cooled, both of which are cumbersome and/or difficult. Other scintillators with better thermal handling capabilities have been suggested (for example, $Y_3Al_5O_{12}(Ce)$ [type P-46]) but they all have a relatively low light efficiency compared to the ZnS(Ag) [type P-11].

VIII. OPTICAL RESOLUTION

We investigated the optical resolution of the detector by using different images at the scintillator location. In Fig. 11 is shown the pitch angle distribution for a thin slit (~0.5-mm wide corresponding to ~2° in pitch angle) which has been lighted from the back. One can observe the effects of the optical broadening, which can be roughly fitted by a Gaussian with a FWHM of 5°. This optical broadening is due to the the lenses, fiber optic bundles, and
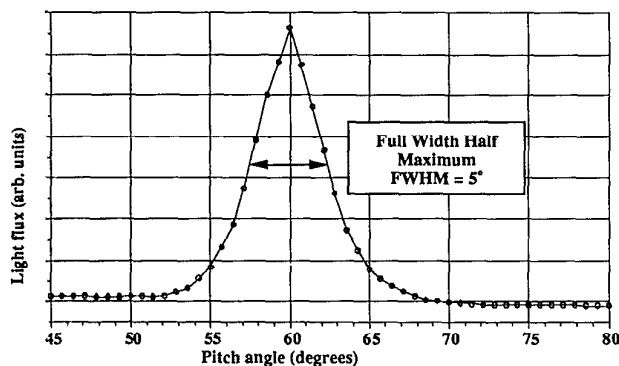

FIG. 11. Test image (thin slit, ≲2° wide) showing the optical broadening due to the various optical components (lenses, fiber optics, camera). The resulting distribution is close to a Gaussian with a FWHM of 5°.

the camera itself. The overall pitch angle resolution, which includes the geometrical resolution from the aperture finite dimensions,[8] is thus of the order of 7° (FWHM). Results shown were obtained for the midplane detector, although similar results were obtained for the bottom detectors.

IX. RADIATION AND OTHER DAMAGES

In the harsh environment inside the first wall of a tokamak, scintillators are exposed to severe conditions which include high radiation levels and possible high temperatures. It is important to understand the consequences of long term exposures to those severe conditions, especially if the access to the diagnostic is restricted to machine openings only (which are usually months apart).

The effects of exposures to large fluence of MeV charged particles have been simulated by putting a source ($\approx 100 \mu Ci$) of 4.5-MeV alphas (^{241}Am) within 1 mm of a scintillator for a continuous period of two months. It was estimated that the scintillator received a flux of approximately 5×10^{12} alphas over an area of approximately 1 cm^2. Part of the scintillator was not exposed to the alphas for a subsequent comparison in light emission. After the two month period, excitation with the same alpha source revealed a drop of 20%–30% from excitation with 4.5-MeV alphas [similarly for P-31 ZnS(Cu)], consistent with damage thresholds found in the literature.[31]

Long term exposures were also monitored by comparing scintillators used on TFTR with unused ones fabricated at the same time but kept away from any radiation sources. The scintillators retrieved from the detectors were exposed during the 1988–89 run period to approximately 12 000 neutral beam heated shots (which give the highest flux of charged fusion products to the scintillator). This number of shots would correspond to approximately 10^{12}-MeV ions (i.e., tritons and protons). Comparison of light emission (using 4.5-MeV alphas) with an unused scintillator showed an averaged light output decrease of less than 10%, although some unexpected arc-like damage pattern was observed.[32]

X. FUTURE WORK

Through this calibration procedure we exposed some problems that needed a special or more elaborate experimental technique. Resolution in the energy and particle species dependence of the scintillation light emission could be improved by using a monoenergetic particle beam (with different species studied separately). The particle's energy would be known accurately, Doppler shift effects would be eliminated, and the scintillator light response dependence could be extended to deuterons and ^3He. Present plans[33] are to use the Van de Graaf accelerator facility at the Los Alamos National Laboratory for species and energy characterization of the scintillator.

Angular dependences proved to be also important in the scintillator characterization and further work is needed for a complete understanding. The linearity of the light emission versus incident flux is still a concern for D-T

operations, although preliminary results which indicate linearity for 4.5-MeV alpha fluxes from 10^5 to 10^7 alphas/s/cm^2.[33]

Finally, it is important to study the effects of radiation and heat on the scintillators. Operations of lost alpha diagnostics, in ITER for example, will be severely limited by their ability of sustaining large stresses due to heat or radiation. Effects of long term exposures remain to be assessed for these types of scintillators.

ACKNOWLEDGMENTS

[1] S. J. Zweben et al., Nucl. Fusion 30, 1551 (1990).

[2] R. L. Boivin, S. Kilpatrick, D. Manos, and S. J. Zweben, Rev. Sci. Instrum. 61, 3208 (1990).

[3] S. J. Zweben, Rev. Sci. Instrum. 57, 1774 (1986).

[4] S. J. Zweben, Nucl. Fusion 29, 825 (1989).

[5] F. A. Kröger, Some Aspects of the Luminescence of Solids (Elsevier, Amsterdam, 1948).

[6] G. F. J. Garlick, Luminescent Materials (Clarendon, Oxford, 1949).

[7] H. W. Leverenz, An Introduction to Luminescence of Solids (Wiley, New York, 1950).

[8] R. L. Boivin, PhD thesis, Princeton University, Princeton, NJ, 1991, also under report PPPL No. 2797.

[9] Thomas Electronics, 100 Riverside Dr., Wayne, NJ 07470.

[10] D. Curie, Luminescence in Crystals (Wiley, New York, 1963).

[11] Phosphor Resource Manual for Industrial and Military Cathode Ray Tubes (published by the Imaging and Sensing Technology Corporation).

[12] W. J. Price, Nuclear Radiation Detection (McGraw-Hill, New York, 1964).

[13] Hamamatsu model R-762.

[14] P. Bayetti, F. Bottiglioni, G. Martin, and J. Paméla, Rev. Sci. Instrum. 57, 62 (1986).

[15] D. Markevich and R. R. Smith, Nucl. Instrum. Methods B 4, 388 (1984).

[16] S. Keszthelyi-Landori and G. Hrehuss, Nucl. Instrum. Methods 68, 9 (1969).

[17] J. B. Czirr, Nucl. Instrum. Methods 25, 106 (1963).

[18] R. L. Craun and D. L. Smith, Nucl. Instrum. Methods 80, 239 (1970).

[19] G. F. Knoll, Radiation Detection and Measurement (Wiley, New York, 1979).

[20] H. H. Andersen and J. F. Ziegler, Hydrogen Stopping Powers and Ranges in all Elemental Matter (Pergamon, New York, 1977), Vol. 3.

[21] J. F. Ziegler, Helium Stopping Powers and Ranges in all Elemental Matter (Pergamon, New York, 1977), Vol. 4.

[22] I. Broser and W. Reichardt, Zeitschrift fur Physik 134, 222 (1953).

[23] S. J. Zweben, Rev. Sci. Instrum. 60, 576 (1989).

[24] Xybion, model ISG-03, rated sensitivity of 10^{-5} footcandle.

[25] Epix, North Brook, IL 60062.

[26] Plexiglass W-2447, 0.62 cm, excellent for making a lambertian (isotropic and uniform) source.

[27] A. Stimson, Photometry and Radiometry for Engineers (Wiley, New York, 1974).

[28] Model 420, Optronic Laboratories, Inc., Orlando, FL 32811.

[29] Xybion model ISG-250.

[30] Z. Lin, Technical Report PPPL-TM-392, December 1991.

[31] J. B. Birks, The Theory and Practice of Scintillation Counting (Pergamon, Oxford, 1964).

[32] S. J. Zweben et al., Rev. Sci. Instrum. 63, Part II October (1992).

[33] M. Tuszewski and S. Zweben, Rev. Sci. Instrum. 63, Part II October (1992).